NASA Technical Memorandum 82704

Creep Shear Behavior of the Oxide Dispersion Strengthed Superalloy MA 6000E

Thomas K. Glasgow
Lewis Research Center
Cleveland, Ohio

Prepared for the
One-hundred-tenth Annual Meeting of the American Institute of Mining, Metallurgical and Petroleum Engineers
Chicago, Illinois, February 22-26, 1981

NASA

CREEP SHEAR BEHAVIOR OF THE OXIDE DISPERSION STRENGTHENED SUPERALLOY MA 6000E

Thomas K. Glasgow

National Aeronautics and Space Administration
Lewis Research Center
Cleveland, Ohio 44135

ABSTRACT

The shear rupture life of the oxide dispersion strengthened (ODS) superalloy MA 6000E was determined at 650° and 760° C using a specimen simulating a gas turbine blade root. The shear stress for 100 hour life at 650° C was 430 MPa and at 760° C was 250 MPa. Comparisons were made at 760° C with the conventional cast superalloy B-1900+Hf, the ODS alloy MA 754, and the directionally solidified eutectic alloy $\gamma/\gamma'-\delta$. The shear stress for 100 hour life at 760° C for MA 754 was 110 MPa, for $\gamma/\gamma'-\delta$ was 170 MPa and for B-1900+Hf was 360 MPa. MA 6000E and $\gamma/\gamma-\delta$ failed with very little indication of ductile accommodation. Both MA 754 and B-1900+Hf showed some ductile tearing. Fracture surfaces of the ODS alloy MA 754 showed discontinuities similar in size, shape, and roughness to its grain structure, but the fracture surfaces of MA 6000E were much smoother than its grain boundaries.

E-985

INTRODUCTION

The strengthening contributions conferred by solid solution, by an oxide dispersion, by gamma prime precipitation, and by a highly elongated microstructure have been successfully combined in the alloy MA 6000E. This oxide dispersion strengthened (ODS) nickel-base superalloy was identified and developed at the International Nickel Company under NASA sponsorship (Refs. 1 and 2). It is manufactured by the mechanical alloying process (Ref. 3). The potential for use of an ODS superalloy as blades in advanced high temperature gas turbine engines has been described (Refs. 4 and 5). In general, the combination of properties possessed by MA 6000E including high temperature strength, good corrosion and oxidation resistance, and superior thermal fatigue resistance render it attractive for gas turbine blade application. It is especially attractive to the designers of the smaller, more difficult to cool engines, where it may find use as a solid (i.e. uncooled) blade.

Several of the mechanical properties of MA 6000E have been determined and reported elsewhere (Refs. 1 and 2). One of the properties which has received little attention, however, is shear strength. Gas turbine blades are fastened to the periphery of disks by a mechanical attachment (variously called dovetail or firtree, Fig. 1). The dovetail must withstand the centrifugal force tending to pull the blade from the rapidly rotating disk. The resulting stress state includes a significant shear stress (Ref. 6) tending to separate the tangs (projections) from the dovetail. When the blade material has microstructural elements such as interfaces or grain

boundaries aligned in the shearing direction, shear deformation can happen along preferred or easy paths. Failure can then occur at loads lower than might be expected from measurement of uniaxial tensile or creep strength. It has been observed (Ref. 7) that in aligned materials of low transverse ductility, the problem is especially severe.

The rationalization of this observation is as follows: testing in transverse tension applies a direct tensile stress to the interface between elongated microstructural elements. If the interface represents a major portion of the specimen cross section, and if the interface has less strength than the balance of the specimen, failure will occur along the interface prior to significant yielding of the material. Weak interfaces are thus reflected in low transverse ductilities. And an interface weak in tension may also be expected to be weak in shear if it is not so convoluted that shear is forced to occur elsewhere. Ductility is also a measure of a material's ability to accommodate initial stress concentrations to make loading more uniform and thereby increase fracture resistance.

The problem of low shear strength in an alloy of aligned microstructure and low transverse ductility was amply illustrated by the directionally solidified eutectic alloy gamma/gamma prime-delta (γ/γ'-δ). This alloy possesses outstanding tensile and creep strength measured in conventional uniaxial tension tests (Ref. 8). However, the shear strength, especially in long term shear rupture tests, was judged inadequate for the root attachment loads imposed in advanced, hollow blade, high work gas turbine engines (Ref. 6). It should be noted that a subsequently developed eutectic alloy, γ/γ'-α, has demonstrated both improved transverse ductility and improved shear strength (Refs. 9 and 10).

Like γ/γ'-δ, MA 6000E has an aligned microstructure (Fig. 2); however the grain boundaries in MA 6000E are distinctly more infrequent and more highly irregular than the interfaces of the directionally solidified eutectic. The transverse ductility of MA 6000E at 760° C is lower than most conventional superalloys, about 2 percent measured as reduction in area of subsize specimens oriented in the short transverse direction (Ref. 11). The short term shear strength of MA 6000E was determined in a previous investigation (Ref. 7). The objective of this study was to determine the longer term or creep shear properties of MA 6000E. Testing was performed at 650° and 760° C, temperatures in the range of expected blade root application. A special specimen, simulating the stress state in a firtree attachment, was employed.

A conventionally cast alloy, B-1900+Hf, was tested as representative of nickel-base superalloys currently used as gas turbine blades. To determine whether the shear behavior of MA 6000E was generic to ODS alloys, MA 754 was also examined. Like MA 6000E, MA 754 is strengthened by a dispersion of fine oxide particles and by an elongated grain structure (Ref. 12). MA 754, however, is a solid solution alloy, not strengthened by the precipitates of gamma prime found in MA 6000E and in B-1900+Hf. Both ODS alloys exhibit crystallographic and mechanical property anisotropy.

In discussion of the results of this study, frequent reference will be made to the behavior of the directionally solidified eutectic alloys, γ/γ'-δ and γ/γ'-α. The γ/γ'-δ alloy is of interest primarily because extensive attention has been given to the shear behavior of this highly anisotropic material (Refs. 6, 8 and 13). Though not tested in this study,

fractured specimens of γ/γ'-δ and γ/γ'-α from previous investigations (Refs. 6 and 10, respectively) were examined.

MATERIALS AND TEST PROCEDURE

The nominal compositions of the alloys MA 6000E, MA 754, and B-1900+Hf are listed in Table I. Also included in Table I are the compositions of carbon modified γ/γ'-δ and of γ/γ'-α. While both MA 6000E and MA 754 had elongated microstructures resulting from hot rolling and recrystallization, the B-1900+Hf tested was a conventionally cast alloy having approximately equiaxed grains of about 2 mm diameter. In previous studies, B-1900 (without added Hf) has been identified an an alloy of high shear strength (Ref. 6).

To evaluate the materials under loading conditions simulating those prevailing in a root attachment, a special specimen, shown in Fig. 3, was devised. The angle between the loading surface and the specimen axis was 135°. The notch radius at the intersection of the tang protrusion and the specimen axis was sharper (r = 0.2 mm) than in an actual turbine blade dovetail (e.g., r = 0.8 mm); this could be expected to give a greater stress concentration. While the choice of a sharp radius to some extent penalized materials of low ductility, it resulted in data that can probably be taken as a lower limit of material behavior or a worst case of dovetail design. The data of Ref. 6 was obtained using a much more complex design more closely simulating a firtree root attachment. It is, therefore, not strictly comparable to the data of this study; it has, however, been taken as representative of the capability of the eutectic alloy γ/γ'-δ in the figures and discussions that follow.

Creep shear tests were performed at 650° and 760° C for MA 6000E and at 760° C for MA 754 and B-1900+Hf. Most testing was performed at stresses chosen to result in creep shear failure after approximately 100 hour lives. All testing was performed in air. While the γ/γ'-δ described in Ref. 6 was given an oxidation resistant coating prior to test, none of the MA 6000E, MA 754, or B-1900+Hf specimens of this study were coated. The specimens of MA 6000E and MA 754 were oriented such that the shearing plane was the rolling plane, see Fig. 4, as it would be in a blade machined from DDS bar material. As in Ref. 6, the applied shear stress was calculated based on an even distribution of stress over the tang shear area parallel to the specimen longitudinal axis. The total shear area was 1 cm^2. Specimens of lamellar γ/γ'-δ and of the more recently developed directionally solidified fibrous eutectic γ/γ'-α (Mo) previously tested (Refs. 6 and 10, respectively) were metallographically examined in addition to those from this program.

RESULTS

Mechanical Test Results

Creep shear results at 760° C for MA 6000E, MA 754, and B-1900+Hf are listed in Table II. Table III shows similar data for MA 6000E tested at 650° C. For convenience in comparing the data from different temperatures, Larson-Miller parameters were calculated using the equation

P = 1.8T (20 + log t) where the temperature, T, is in °K and the time to failure, t, is in hours. A plot of creep shear data of this study and data from Ref. 6 for γ/γ'-δ is given in Fig. 5. Parameter values for 100 hour lives at 650° and 760° C, P = 36.6 and 40.9, respectively, have been marked on the abscissa. Also plotted in Fig. 5 are calculated shear stresses for a specific large hollow (cooled) blade and a range of shear stress characterizing modifications of a small solid blade (Ref. 13).

As shown in Fig. 5, the alloy of highest shear rupture capability was B-1900+Hf. Most of the B-1900+Hf data were obtained at 350 MPa to establish confidence in a value representing its 760° C 100 hour shear rupture strength. Some of the B-1900+Hf specimens tested at higher loads failed as in notched conventional rupture tests, i.e. non-shear failures (see Table II). Those tests of B-1900+Hf conducted at much lower stresses were terminated to avoid inordinately long test times. The 760° C, 100 hour shear rupture capability of B-1900+Hf determined in this study was 360 MPa.

The shear rupture data for MA 6000E are represented as a band in Fig. 5 lying well above that for γ/γ'-δ, but below that of B-1900+Hf. The 760° C, 100 hour shear rupture strength of MA 6000E was 250 MPa. While the shear rupture data from Ref. 6 for γ/γ'-δ fall well below that of MA 6000E, an exact comparison cannot be made because the test specimens differed. The indicated 760° C, 100 hour shear strength of γ/γ'-δ was 170 MPa. The lowest shear rupture capability, 110 MPa at 760° C for 100 hours, was exhibited by MA 754.

MA 6000E exhibited a sharp temperature dependence of shear rupture strength (compare Tables II and III). At 650° C, the average 100 hour shear rupture stress was 430 MPa and at 760° C, was 250 MPa, a decrease proportionate to the decrease in stress for stress rupture failure of conventional nickel-base superalloys over the same temperature range. This is an indication that the measured shear properties of MA 6000E are largely controlled by conventional gamma prime precipitation, a temperature sensitive strengthening mechanism over the range 650° to 760° C.

A graphic comparison of each alloy's shear rupture strength to its uniaxial tension rupture strength is given in Fig. 6 as the ratio shear divided by tensile rupture strength. The rupture strengths of B-1900+Hf, MA 6000E, MA 754, and γ/γ'-δ were taken from Refs. 14 (extrapolation), 1, 15, and 8, respectively. The ratios of shear to uniaxial tension rupture strength ranged from a low of 25 percent for γ/γ'-δ to a high of 55 percent for B-1900+Hf. The latter value is about the expected ratio for an isotropic material.

Microstructural Results

Metallographically prepared cross-sectional views of sheared specimens are shown in Fig. 7. The fracture of MA 6000E, Fig. 7(a), proceeded along rather straight lines with some segments exactly parallel to the working direction, but more generally at a slight angle; little evidence of deformation was observed. In contrast, the fracture of MA 754, Fig. 7(b), was irregular, showing segments which followed grain boundaries and other areas that were heavily deformed. The fracture of B-1900+Hf, Fig. 7(c), proceeded transgranularly along straight lines with steps at carbide particles or at eutectic nodules. Specimens, of γ/γ'-δ from the study described in

Ref. 6, were examined. The less ductile reinforcing Ni_3Cb or delta phase appears as solid light gray lammellae in Fig. 7(d). The preferred shear fracture path was either through the δ phase or alternatively along the interface between the δ phase and the γ/γ' lamellae.

Fracture surfaces were also examined and are shown in Fig. 8. Largely planar surfaces, much smoother than the grain boundaries, were evident in MA 6000E, Fig. 8(a). The parallel alignment of fracture segments having the appearance of cleavage suggested crystallographic control of the fracture path. Similarly faceted fractures have been observed in conventional nickel-base alloys tested in stress rupture at 650° C (Ref. 16) and in tension at 704° C (Ref. 17). Reference 17 attributes this type of fracture in Inconel X-750 to observed channeling of all dislocation activity through narrow slip bands in this temperature range.

Rough twisted and torn surfaces were observed in MA 754, Fig. 8(b). A combination of ductile tearing and cleavage type fractures characterized B-1900+Hf, Fig. 8(c). Its fracture surface was considerably rougher than that of MA 6000E. The only ductility evident in the γ/γ'-δ specimens was in the tearing of the oxidation resistance coating applied to its surface, Fig. 8(d). Similar observations at higher magnification were made by scanning electron microscopy. MA 6000E, MA 754, B-1900+Hf, and γ/γ'-δ are shown in Figs. 9(a) to (d) respectively. Also available was a specimen of the ductile phase (Mo) reinforced eutectic alloy γ/γ'-α from the investigation reported in Ref. 10. Its fracture appearance, see Fig. 10, was very similar to that of γ/γ'-δ, Fig. 9(d), with the exception of the presence of a few bent fibers or fiber bundles. The fracture path observed in metallographically prepared cross sectional views was preferentially along the α fiber γ/γ' matrix interface.

DISCUSSION

Rationalization of the Shear Rupture Data

The levels of shear rupture capability found in this study and in Ref. 6 may be rationalized by considering the normalized shear rupture strengths of the alloys, their microstructures, and their fracture characteristics. Figure 6 presents the ratios of shear to uniaxial tension rupture stength for the four alloys.

The two ductile alloys, B-1900+Hf and MA 754, attain in shear half or more of their tensile rupture capability. They should be considered similar in their shear rupture behavior although the absolute values of shear strength differ widely. Each showed evidence of ductile yielding, though the fracture of B-1900+Hf was transgranular while that of MA 754 was primarily intergranular. The substantial transverse ductility of MA 754 and the rough interlocking nature of its grain boundaries allowed it to sustain a high shear load relative to its tensile rupture strength.

There was an important difference between the two less ductile alloys MA 6000E and γ/γ'-δ. The transgranular fracture mode of MA 6000E promoted by the roughness and paucity of its grain boundaries resulted in shear rupture fracture at a relatively high fraction, 0.45, of its tensile rupture strength. The abundant smooth interfaces aligned in the direction of shear-

ing led to shear failure of γ/γ'-δ at a low fraction, 0.25, of its uniaxial tension rupture strength.

The relatively high ratio of shear/tensile strength and the generally transgranular fracture exhibited by MA 6000E suggest that efforts to improve shear capability by modifying or eliminating the grain boundaries would not be fruitful. Rather, the basic strength of the alloy and its ductility should be improved. Strength at root application temperatures could be affected by alloy changes and possibly by post recrystallization thermomechanical processing. Ductility might be improved by decreasing the total content of dispersed hard phase including oxides, nitrides, and carbides, which in the current alloy total about four volume percent.

Suitability of MA 6000E for Root Application

Very little data concerning actual levels of shear stress in current blade attachments were found in the literature, and the stress levels in future engines are not yet defined. The data, which were found, are indicated in Fig. 5 as a single line for a particular large hollow blade considered in Ref. 6, and a range of stress for a variety of root configurations of a small solid blade (Ref. 13). Perhaps the most interesting point is that depending on the root design, the shear stress may vary widely for the same airfoil; this is shown by the width of the band in Fig. 5.

The data for MA 6000E indicate that it could serve well as a small solid blade under the conditions of stress described in Ref. 13. The intersection of the stress level in a large hollow blade and the lower edge of the MA 6000E data band in Fig. 5 occurs at a Larson-Miller parameter indicating only a few hundred hours life at 760° C. This rather marginal result indicates that care must be taken in the choice of root design to be used with this alloy as a large hollow blade. It also suggests the attractiveness of bonding a conventional superalloy, e.g., B-1900+Hf, root to a MA 6000E airfoil for cases in which the shear stress cannot be decreased by altered design. Finally, it can be recommended that before efforts are undertaken specifically to improve the shear strength of MA 6000E, actual shear stress levels be identified for current and anticipated cooled gas turbines.

SUMMARY OF RESULTS AND CONCLUSIONS

The shear rupture capability of the oxide dispersion strengthened superalloy MA 6000E, a potential gas turbine blade material, has been examined in comparison with the alloys MA 754, B-1900+Hf, and γ/γ'-δ. Tests of the alloy in root attachment configuration (dovetail) have led to the following results and conclusions:

1. At 650° C, the shear stress for 100 hour life of MA 6000E was 430 MPa, and the estimated shear stress for 1000 hour life was 360 MPa.
2. At 760° C, the shear stress for 100 hour life was 250 MPa, and the stress for an estimated 1000 hour life was 180 MPa.
3. The temperature dependence of shear rupture life in MA 6000E was similar to the temperature dependence of uniaxial tension rupture life for conventional nickel-base superalloys indicating strength control by the precipitated phase, gamma prime.

4. The stresses for 100 hour life at 760° C of B-1900+Hf, $\gamma/\gamma'-\delta$, and MA 754 were 360, 170, and 110 MPa, respectively.

5. Two ODS alloys showed different shear fracture behavior. The shear fracture of MA 6000E occurred with little evident ductility along largely planar surfaces (assumed crystallographic), while MA 754 exhibited substantial ductile tearing and fracture along grain boundaries. The behavior of B-1900+Hf was intermediate. Two directionally solidified eutectic alloys, $\gamma/\gamma'-\delta$ and $\gamma/\gamma'-\alpha$ (Mo) both showed failure along the reinforcing phase interface.

6. The oxide dispersion strengthened superalloy MA 6000E shows considerably greater shear capability than the eutectic alloy $\gamma/\gamma'-\delta$, and appears to have sufficient strength for some solid blade designs without alloy modification. Examination of the calculated shear stress levels in highly stressed, cooled blade root designs should precede efforts undertaken specifically to improve MA 6000E shear properties.

7. If required, improvement of either or both the ductility and the 760° C strength could be expected to increase the shear rupture capability of MA 6000E.

REFERENCES

1. H. F. Merrick, L. R. R. Curwick, and Y. G. Kim: NASA CR-135150, January 1977.
2. Y. G. Kim and H. F. Merrick: NASA CR-159493, May 1979.
3. J. S. Benjamin: Met. Trans., 1970, vol. 1, pp. 2943-2951.
4. J. S. Benjamin: ASME Paper 76-GT-118, March 1976.
5. T. K. Glasgow: NASA TM-79088, 1979.
6. K. D. Sheffler and J. J. Jackson: NASA CR-135005, December 1976.
7. T. K. Glasgow: NASA TM-78973, 1978.
8. K. D. Sheffler, R. H. Barkalow, J. J. Jackson, and A. Yuen: NASA CR-135000, May 1976.
9. M. F. Henry, M. R. Jackson, M. F. X. Gigliotti, and P. B. Nelson: NASA CR-159416, January 1979.
10. F. H. Harf: In Conference on In-Situ Composites - III, J. L. Walter, M. G. Gigliotti, D. F. Oliver, and H. Bibring, eds., p. 399, Ginn Custom Publishing, Lexington, MA, 1979.
11. A. E. Anglin, Jr.: NASA TM-79189, 1979.
12. "Inconel Alloy MA 754," Alloy Digest, Ni-244, May 1977.
13. A. D. Cetel and M. Gell: PWA-5530-4, Pratt and Whitney Aircraft, West Palm Beach, FL, May 1978. (AD-B029155L)
14. High Temperature, High Strength Nickel-Base Alloys, 2nd ed., The International Nickel Company, Inc., New York, A-393, 1964.
15. T. E. Howson, D. A. Mervyn, and J. K. Tien: Met. Trans. A, 1980, vol. 11A, pp. 1609-1616.
16. M. N. Menon and W. H. Reimann: AFML-TR-74-100, Air Force Materials Lab., Wright-Patterson AFB, OH, October 1974.
17. W. J. Mills: Met. Trans. A, 1980, vol. 11A, pp. 1039-1047.

TABLE I. - NOMINAL COMPOSITIONS OF ALLOYS EXAMINED IN CREEP SHEAR, WEIGHT PERCENT

Alloy	Ni	Cr	Co	Mo	W	Ta	Cb	Hf	Al	Ti	C	B	Za	Y_2O_3
MA 6000E	Bal.	15	--	2	4	2	----	---	4.5	2.5	0.05	0.01	0.15	1.1
MA 754	Bal.	20	--	--	-	--	----	---	.3	.5	.05	-----	----	.6
B 1900+Hf	Bal.	8	10	6	-	4	----	1.2	6	1	.12	.013	.05	---
$\gamma/\gamma'-\delta$	Bal.	6	--	--	-	--	20.1	---	2.5	---	.06	-----	----	---
$\gamma/\gamma'-\alpha$	Bal.	--	--	33	-	--	----	---	5.7	---	----	-----	----	---

TABLE II. - SHEAR RUPTURE LIVES OF MA 754, MA 6000E, AND B-1900+Hf DETERMINED WITH SIMULATED ROOT SPECIMENS AT 760° C

Alloy	Stress		Life, hr	Larson-Miller parameter, P[a]
	MPa	ksi		
MA 754	100	14.5	[b]381+	42+
	100	14.5	[b]570+	42.3+
	125	18.1	28.4	39.9
	125	18.1	35.3	40.0
	150	21.8	2.5	37.9
	150	21.8	4.8	38.4
MA 6000E	200	29.0	494.4	42.2
	200	29.0	923.4	42.7
	250	36.3	58.6	40.5
			89.1	40.8
			97.7	40.9
			208.9	41.5
			[c]226.0	41.6
			328.8	41.9
	300	43.5	11.2	39.1
			15.3	39.4
			22.1	39.7
			24.3	39.8
			39.3	40.1
			50.0	40.3
B-1900+Hf	200	29.0	[b]2164+	43.4+
	250	36.3	[b]1393+	43.0+
	300	43.5	582.7	42.3
	325	47.1	[d]1.0	-----
	325	47.1	[e]222+	41.6+
	350	50.8	79.4	40.7
			130.0	41.1
			159.1	41.3
			169.5	41.4
			178.6	41.4
	400	58.0	[d]4.9	38.5+
	450	65.3	[d]1.3	37.3+
	500	72.5	0.4	36.4

[a]$P = 1.8\ T\ ^{\circ}K\ (20 + \log t_R) \cdot 10^{-3}$.
[b]Test discontinued.
[c]Mixed tensile and shear failure mode.
[d]Tensile mode failure.
[e]Load train failure.

TABLE III. - SHEAR RUPTURE LIFE OF MA 6000E DETERMINED WITH SIMULATED ROOT SPECIMEN AT 650° C

Stress		Life, hr	Larson-Miller parameter, P[a]
MPa	ksi		
300	43.5	[b]573+	37.8+
350	50.8	436.7	37.6
350	50.8	549.5	37.8
400	58.0	117.7	36.7
400	58.0	241.5	37.2
400	58.0	638.4	37.9

[a]$P = 1.8\ T\ ^{\circ}K\ (20 + \log t_R\ hr) \cdot 10^{-3}$.
[b]Test discontinued.

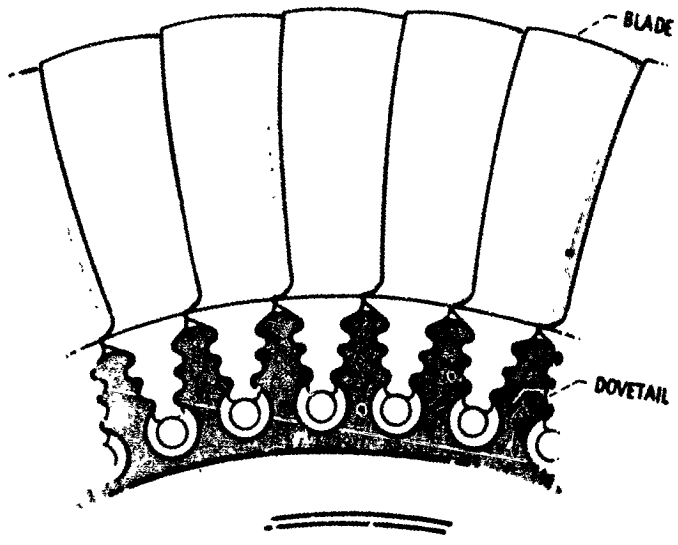

Figure 1. - Dovetail mechanical joint between gas turbine disk and blade.

Figure 2. - Microstructure of the oxide dispersion strengthened superalloy MA 6000E.

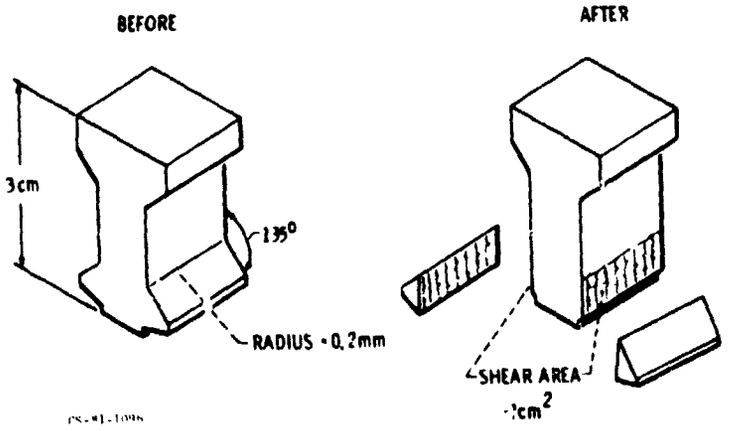

Figure 3. - Test specimen configuration, before and after shearing.

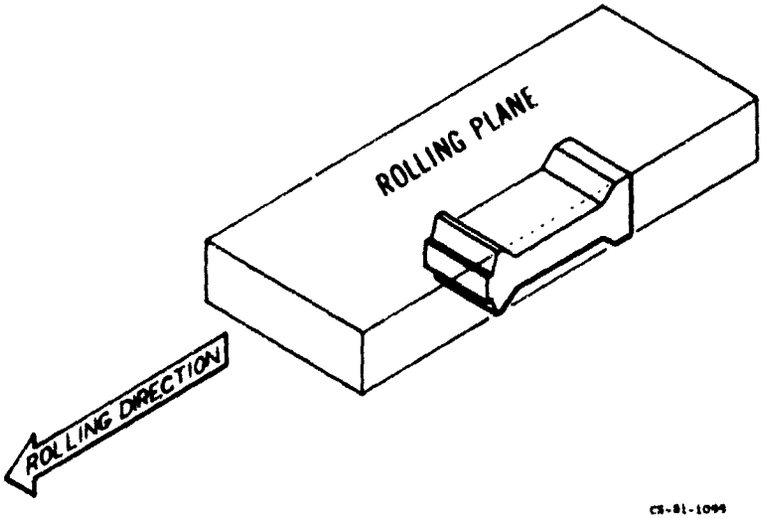

Figure 4. - Creep shear specimen orientation with respect to the rolling direction and rolling plane of MA 6000E and MA 754.

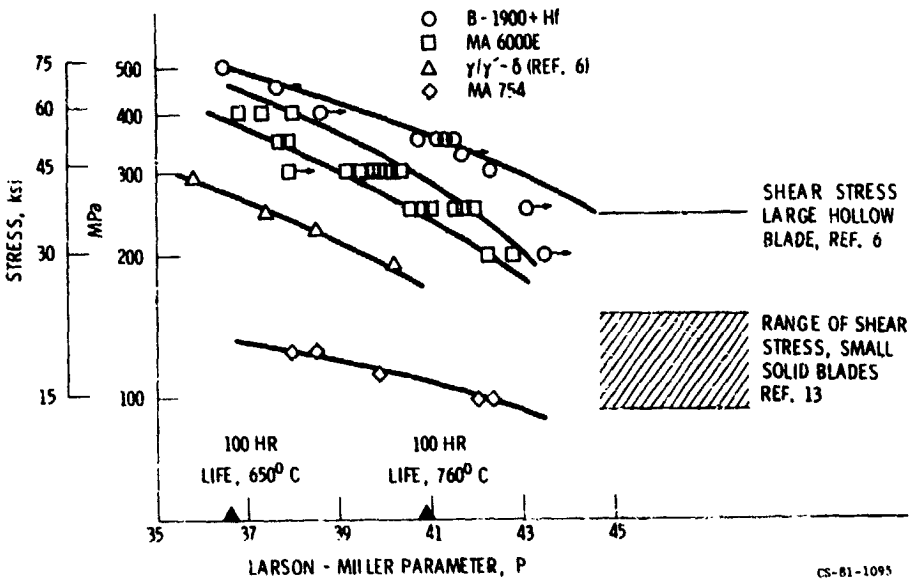

Figure 5. - Results of simulated root attachment shear rupture tests.

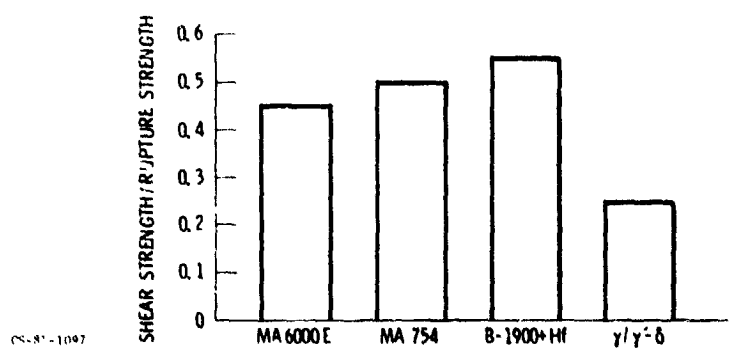

Figure 6. - Ratio of 100 hour 760° C shear rupture strength to uniaxial tension rupture strength.

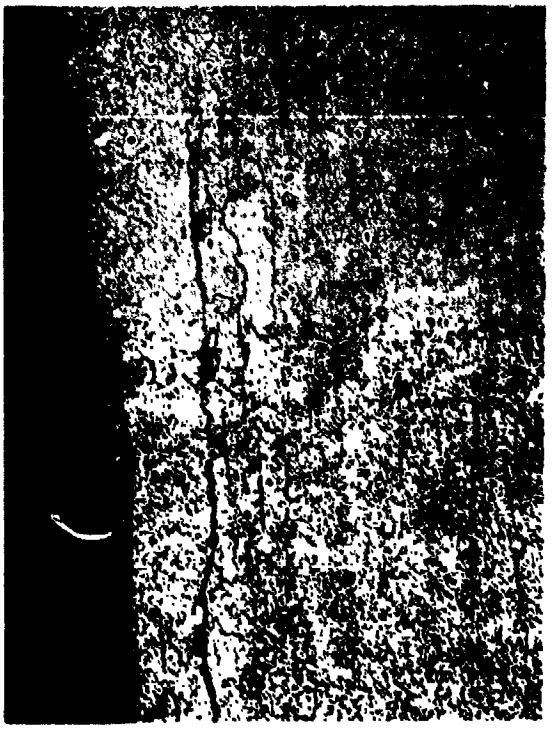

(a) MA 6000.

(b) MA 754.

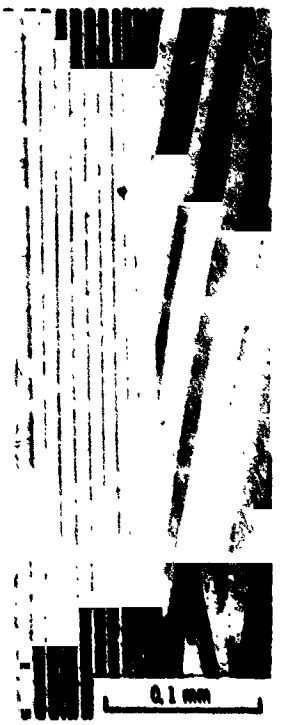

(c) B-1900+Hf.

(d) γ/γ′ - δ.

Figure 7. - Metallographically prepared cross-sectional views of shear rupture surfaces.

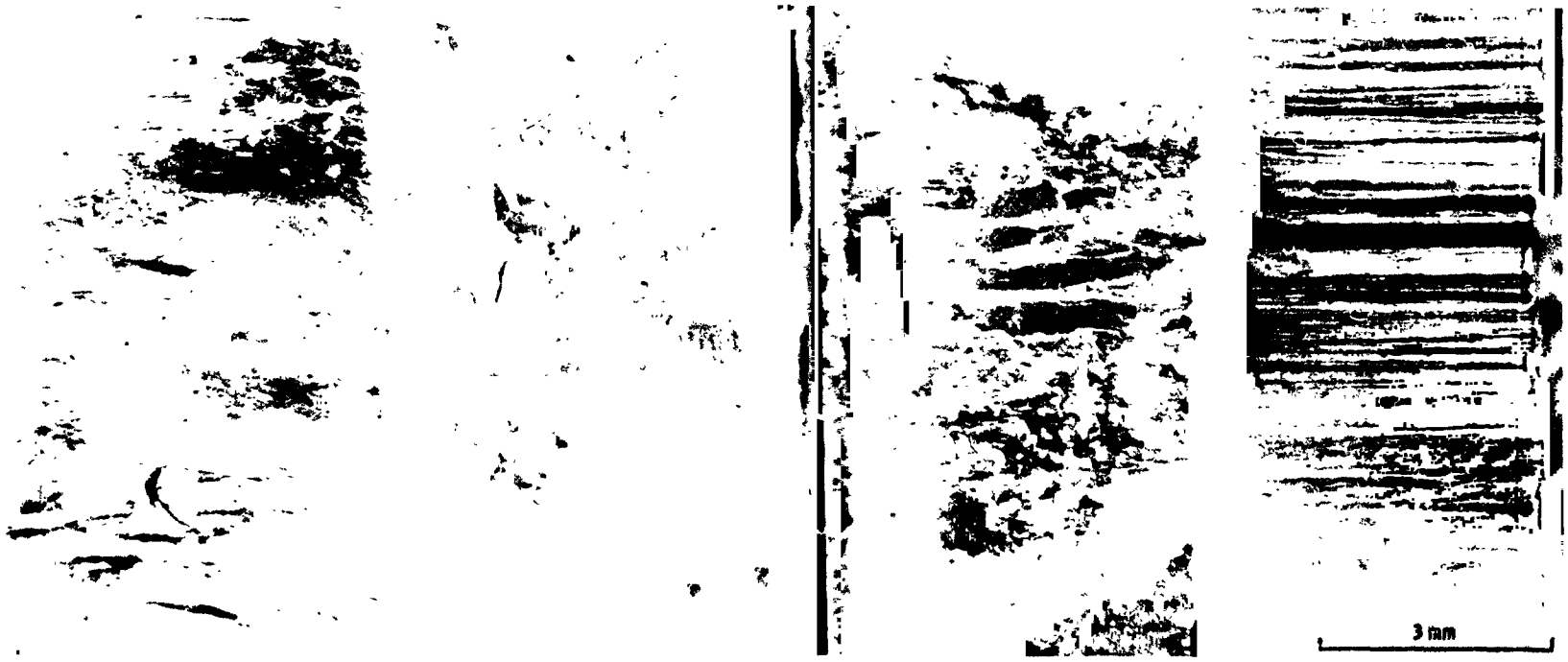

(a) MA 6000E. (b) MA 754. (c) B-1900+Hf. (d) γ/γ' - δ.

Figure 8. - Creep shear fracture surfaces as viewed by light microscopy.

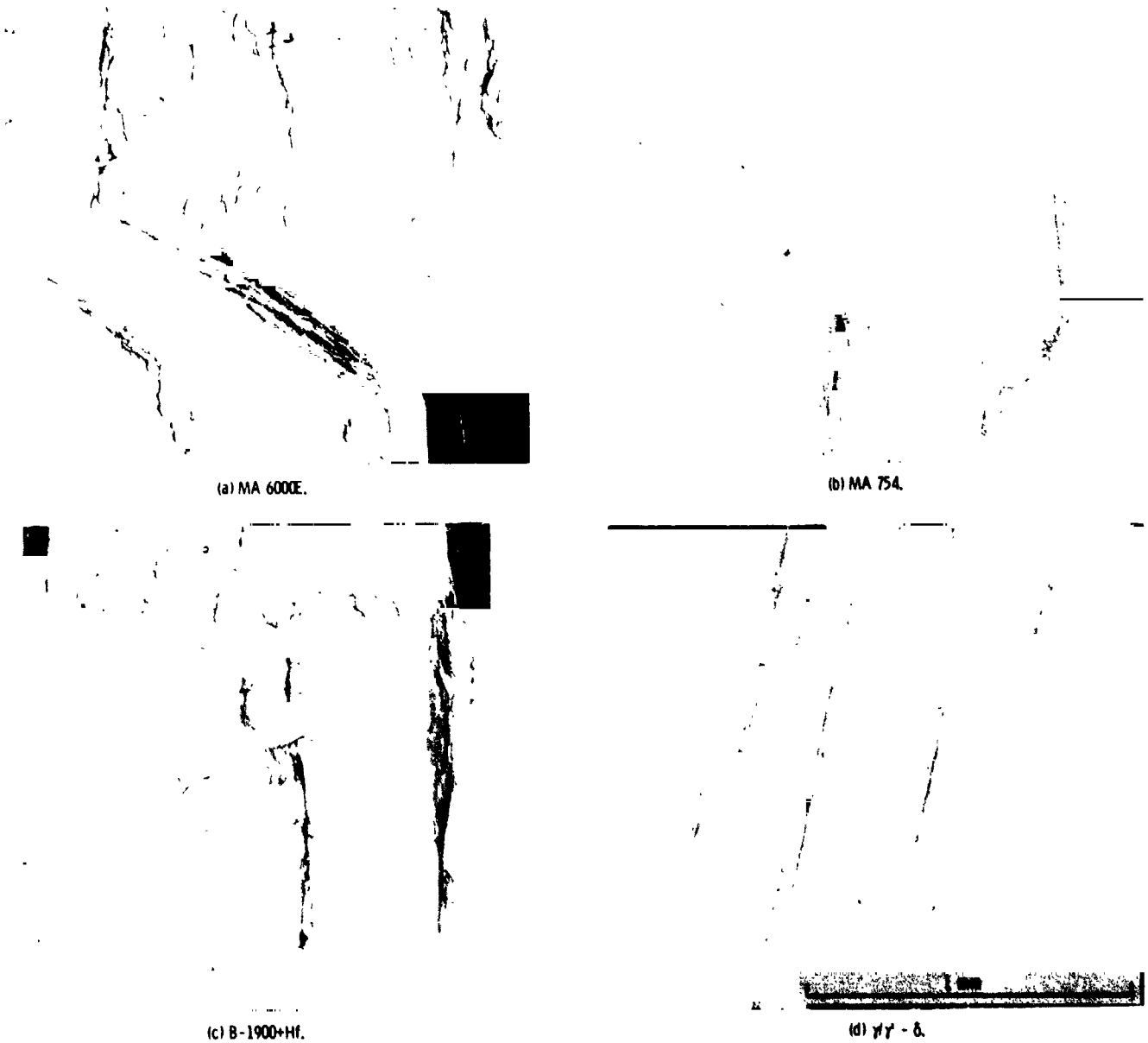

(a) MA 6000E.

(b) MA 754.

(c) B-1900+Hf.

(d) γ/γ' - δ.

Figure 9. - Creep shear fracture surfaces as viewed by scanning electron microscopy.

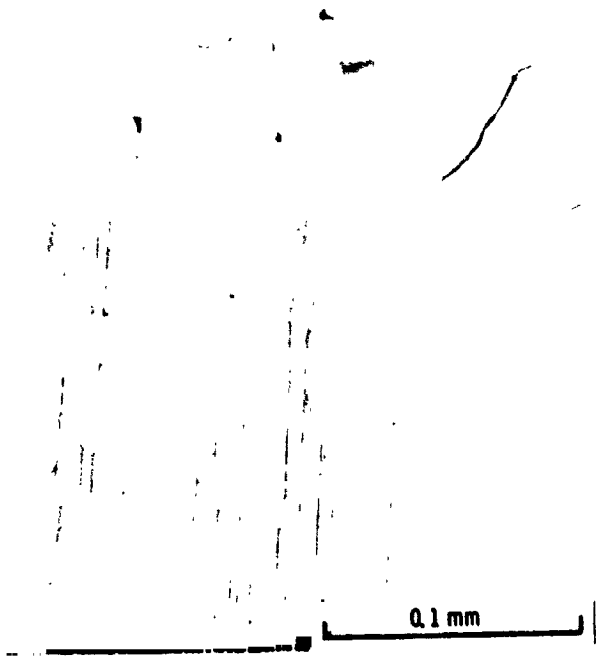

Figure 10. - Shear fracture surface of γ' - α (Mo), bolt head specimen from reference 10.